Conformational Nanobodies Reveal Tethered Epidermal Growth Factor Receptor Involved in EGFR/ErbB2 Predimers

Damien Nevoltris,[†,‡,§,∥,⊥] Benjamin Lombard,[†,‡,§,∥] Elodie Dupuis,[⊥] Gérard Mathis,[⊥] Patrick Chames,[*,†,‡,§,∥,#] and Daniel Baty[†,‡,§,∥,#]

[†]Institut National de la Santé et de la Recherche Médicale, U1068, Centre de Recherche en Cancérologie de Marseille, Marseille F-13009, France, [‡]Aix-Marseille Université, Marseille F-13284, France, [§]Centre National de la Recherche Scientifique, UMR7258, Centre de Recherche en Cancérologie de Marseille, Marseille F-13009, France, [∥]Institut Paoli-Calmettes,F-13009 Marseille, France, and [⊥]Cisbio Bioassays, BP 84175, F-30200 Codolet, France. [#]P.C. and D.B. are senior coauthors.

ABSTRACT The epidermal growth factor receptor (EGFR) is a cell-surface receptor with a single transmembrane domain and tyrosine kinase activity carried by the intracellular domain. This receptor is one of the four members of the ErbB family including ErbB2, ErbB3, and ErbB4. Ligand binding, like EGF binding, induces a conformational rearrangement of the receptor and induces a homo/hetero dimerization essentially with ErbB family receptors that leads to the phosphorylation of the kinase domain, triggering a signaling cascade. EGFR can also form inactive dimers in a ligand-independent way through interactions between cytoplasmic domains. To date, the conformation of EGFR extracellular domain engaged in these inactive dimers remains unclear. In this study, we describe the successful selection and characterization of llama anti-EGFR nanobodies and their use as innovative conformational sensors. We isolated three different specific anti-EGFR clones binding to three distinct epitopes. Interestingly, the binding of all three nanobodies was found highly sensitive to ligand stimulation. Two nanobodies, D10 and E10, can only bind the ligand-free EGFR conformation characterized by an intramolecular tether between domains II and IV, whereas nanobody G10 binds both ligand-free and ligand activated EGFR, with an 8-fold higher affinity for the extended conformation in the presence of ligand. Here we took advantage of these conformational probes to reveal the existence of tethered EGFR in EGFR/ErbB2 predimers. These biosensors represent important tools allowing the determination of EGFR conformations and should help the design of relevant inhibitors.

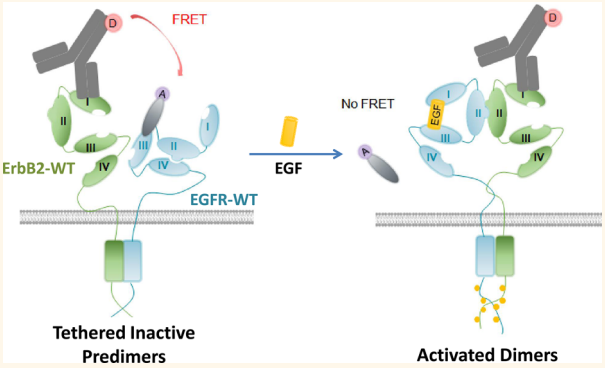

KEYWORDS: phage display · epidermal growth factor receptor (EGFR) · single domain antibodies · nanobodies · conformational changes · biosensors · homogenous time-resolved fluorescence

The epidermal growth factor receptor (EGFR, also called ErbB1 or HER1) belongs to the family of single transmembrane domain receptors with tyrosine kinase activity driven by their intracellular domain. The EGFR family also includes ErbB2, ErbB3, and ErbB4 receptors. The extracellular domain of these receptors presents a ligand-binding site. The binding of a specific ligand induces the receptor activation, ultimately triggering signal transduction pathways involved in cell proliferation, migration, differentiation, and survival.[1] In addition to EGF itself, 11 different ligands have been shown to activate those receptors (including TGF-α, β-cellulin, and neuregulins).[2] ErbB1 is activated by all ligands of this family except neuregulins, specific for ErbB3 and ErbB4. These ligands bind to the extracellular domain of the receptor, inducing a major conformation change. This new conformation allows the formation of homodimers or induces the formation of heterodimers with other members of the family.[3] The structural basis for ligand-induced dimerization of ErbB extracellular regions, which leads to an allosteric activation of the intracellular tyrosine kinase domain, is now well understood.[4−9] However, although ligand binding and

* Address correspondence to patrick.chames@inserm.fr.

Received for review October 9, 2014 and accepted January 20, 2015.

Published online January 20, 2015
10.1021/nn505752u

dimerization events seem connected, several studies have demonstrated that EGFR can also be found on the cell surface as nonactivated dimers, also called predimers.[10−13] Ligand-independent EGFR/ErbB2 dimer formation was shown to require the cytoplasmic domain of EGFR to be present on resting cells.[14,15] The relationship between extracellular regions, transmembrane domains, intercellular juxtamembrane domains, and cytoplasmic tyrosine kinase of ErbB family receptors plays a major role in the dimerization and activation events.[16] Moreover, conformational changes during these activations appear to be key for the signal transduction. Because these inactive predimers are proposed to be primed for ligand binding and allow a fast and efficient signaling, they might represent a very relevant therapeutic target for small inhibitors. Unfortunately, despite the large amount of structural and functional data concerning the various states of EGFR, the conformation of its extracellular domain within predimers has never been captured by crystallography studies and remains largely unknown. Therefore, a precise monitoring of EGFR conformational changes appears crucial to thoroughly understand EGFR family signaling and help in the design of small-molecule drugs. Besides crystallography, other powerful methods such as nuclear magnetic resonance[17] or electron microscopy are increasingly used to solve high quality structures[18] but remain cumbersome and cannot be used on intact cells. Other methods are based on the use of mutant or fusion proteins,[19,20] but they also cannot be used on cells naturally expressing the wild-type receptor. Molecular dynamics simulations[21] can provide essential insights, but as any *in silico* prediction tools, they require an experimental validation of the findings.

Recently, the use of nonconventional antibodies has emerged as a simple, new, and sensitive approach to study protein conformation on living cells. Single domain antibodies (sdAbs, also called nanobodies),[22] correspond to the variable domains of a special class of antibodies naturally devoid of light chains found in camelids. These small proteins (15 kDa) present several advantages[23] including a good thermal stability even without disulfide bond formation,[24] a good solubility, and high expression yield.[25] Most importantly, nanobodies have a natural tendency to bind epitopes that are inaccessible to conventional antibodies,[26] such as cleft and cavities. Consequently, they are often very sensitive to conformational changes of their target.[27,28]

In this study, we have generated and extensively characterized anti-EGFR nanobodies, and taking into account new developments of time-resolved fluorescence resonance energy transfer (TR-FRET) technology,[29] we have demonstrated their ability to sense EGFR conformational changes and highlighted their usage as biosensors to study the conformation of EGFR engaged in EGFR/ErbB2 heterodimers on the surface of cells.

RESULTS

Selection of Nanobodies Displaying High Specificity and Affinity for EGFR. Five anti-EGFR nanobodies were isolated from the repertoire of immunized llamas by alternating phage display selections on recombinant EGFR−human Fc fusion protein and epidermoid carcinoma tumor cell line A431. Preliminary data demonstrated that three of them were targeting a shared epitope (data not shown). Clone E10, chosen as a representative clone of this family, and clones D10 and G10, displaying different sequences, were produced and purified for further characterization. Their binding on all ErbB family members was assayed by ELISA on chimeric recombinant proteins (Figure 1A). These results demonstrated that all nanobodies were highly specific to EGFR.

To confirm the specificity of these clones, similar experiments were conducted using homogenous time-resolved fluorescence[30] (HTRF) on transfected cells (Figure 1B). HTRF combines FRET technology with time-resolved measurement of fluorescence (TR-FRET), allowing elimination of short-lived background fluorescence, thanks to the natural long-lived fluorescences of the terbium-based donor (Lumi4-Tb). For receptor labeling, we used SNAP-tag (ST) or HaloTag (HT),[31−33] which are small fusion proteins (26 kDa and 33 kDa, respectively) that covalently interact with their respective substrates coupled with the donor fluorochrome. Nanobodies were either covalently coupled to an acceptor fluorochrome (called d2) or indirectly detected using a d2-conjugated anti-6His tag monoclonal antibody (mAb). Under these conditions, only a close proximity between the antibody and the receptor leads to an energy transfer, allowing the detection of a specific binding in the absence of washing. This combination between HTRF and SNAP-tag (ST) or HaloTag (HT) technologies is called Tag-lite.

HTRF experiments performed on HEK293T cells transfected with all ErbB family receptors fused to ST or HT confirmed the ability of anti-EGFR nanobodies to specifically bind their antigen in the cell membrane context (Figure 1B). d2-Labeled anti-tag monoclonal antibodies (mAbs) (FLAG-d2 or c-myc-d2) were used to control the membrane expression of all receptors. The apparent affinity of the anti-EGFR nanobodies for their target was measured by HTRF using living cells. The measured affinities of nanobodies for EGFR-ST transfected HEK293T cells were 7, 20, and 12 nM for D10, E10, and G10, respectively (Figure 1C). In this experiment, nanobodies were detected using an anti-6His tag-d2 mAb. To avoid the possible influence of the detection antibody on the dissociation constant measurement, nanobodies were directly coupled with a fluorochrome, and affinity experiments were performed in the same conditions (Table 1). Surprisingly, D10-d2, E10-d2,

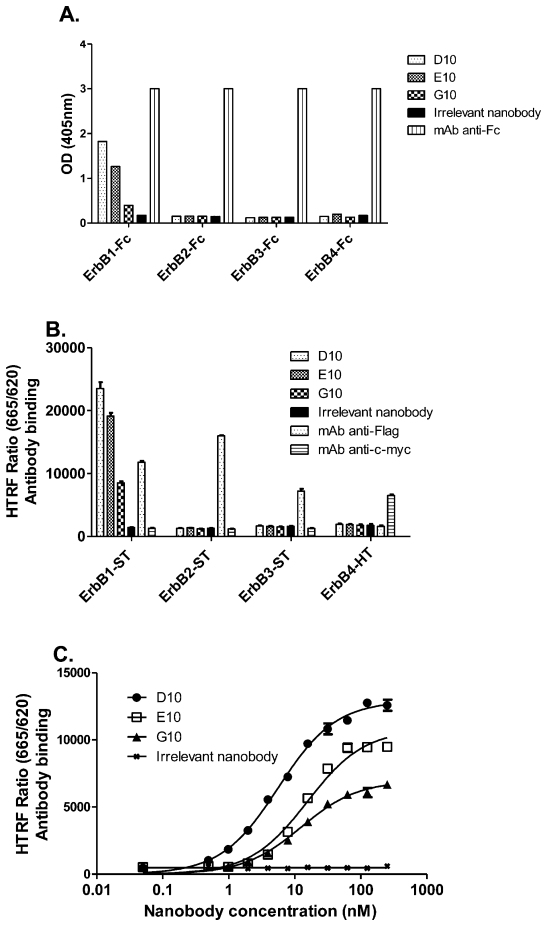

Figure 1. Anti-EGFR nanobodies specificity and affinity. (A) Specificity of anti-EGFR nanobodies D10, E10, and G10 on recombinant proteins by ELISA. ErbB family members fused to a human Fc fragment were adsorbed on plastic plate. Bound nanobodies were detected using a mouse anti-6His mAb followed by a goat anti-mouse-HRP. An anti-Fc mAb was used as a positive control. (B) Specificity of anti-EGFR nanobodies on transfected HEK293T cells by HTRF. HEK293T cells were transfected with plasmid ErbB1-ST (SNAP-Tag (Flag tagged)), ErbB2-ST, ErbB3-ST, ErbB4-HT (HaloTag (c-myc tagged)). Each receptor was covalently labeled with a donor fluorochrome via their ST or HT. Nanobodies were incubated with transfected cells and detected using anti-6His-d2 (acceptor). TR-FRET signal represented by the normalized ratio (665/620) indicates an energy transfer between donor (on receptor) and anti-6His-d2. A mouse anti-Flag mAb or an anti-c-myc mAb were used to measure ErbB1, 2, and 3-ST and ErbB4-HT expression, respectively. (C) Affinity of anti-EGFR antibodies on transfected HEK293T cells determined by HTRF. HEK293T cells were transfected with plasmid ErbB1-ST and labeled by donor fluorochrome. Various concentrations of nanobodies were incubated with cells and detected using acceptor-labeled anti-6His mAb. Apparent K_d was determined by GraphPad. Standard deviations represent three different experiments performed in triplicate.

and G10-d2 displayed slightly higher apparent K_d of 27, 106, and 87 nM, respectively. These small discrepancies could be explained by a partial denaturation of the nanobodies due to the modification of lysine residues by the NHS-d2 fluorochrome or steric hindrances induced by N-terminal labeling next to the antigen binding site. Nevertheless, both approaches

TABLE 1. Affinity Values (K_d, nM) of Unlabeled and d2-Labeled Anti-EGFR Nanobodies Measured by HTRF on EGFR-ST

	D10	E10	G10
unlabeled clone	7	20	12
d2-labeled clone	27	106	87

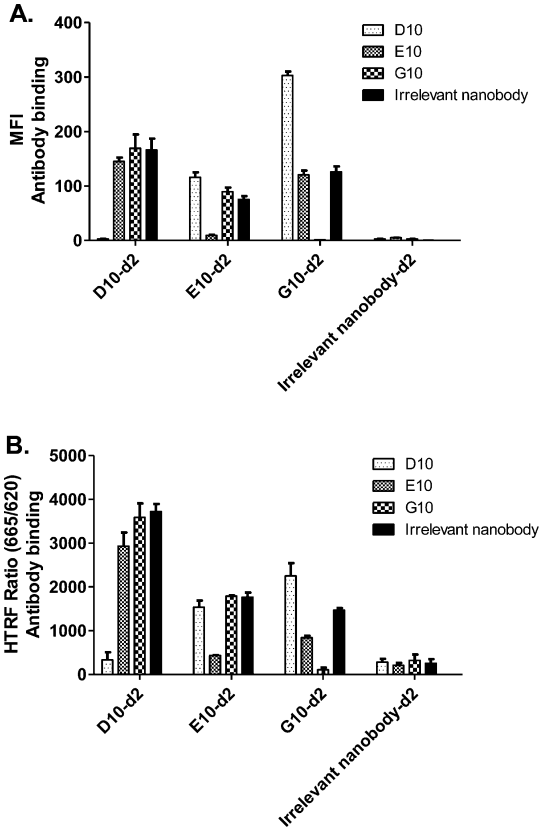

Figure 2. Competition between anti-EGFR nanobodies D10, E10, and G10. (A) Competition of three anti-EGFR nanobodies by flow cytometry. Unlabeled nanobodies and d2-labeled nanobodies were incubated together with A431 cells during 2 h, washed, and analyzed on a flow cytometer. MFI = mean fluorescence intensity. (B) Competition of the nanobodies performed by HTRF. HEK293T cells were transfected with EGFR-ST and labeled with donor (Tb), and nanobodies were incubated during 2 h before reading on fluorescence spectrophotometer. In both experiments, 50 μM unlabeled nanobodies were added, and an irrelevant anti-ErbB2 nanobody was used as negative control. Standard deviations represent three different experiments performed in triplicate.

confirmed that these monovalent binders could bind their target with high affinity.

Anti-EGFR Nanobodies Target Three Distinct Epitopes and Do Not Bind to the Ligand Binding Site. Although the anti-EGFR nanobodies displayed very different variable CDRs (Figure S1, Supporting Information), they did not necessarily bind distinct epitopes. To establish this fact, competition experiments were performed using labeled nanobodies and unlabeled nanobodies using flow cytometry (Figure 2A) and HTRF experiments (Figure 2B). In both techniques, all three

TABLE 2. Affinity Values (K_d, nM) of Anti-EGFR Nanobodies in the Presence of Other Nanobodies as Measured by HTRF (EGFR-ST)

	competitors			
clones	irrelevant nanobody	D10	E10	G10
D10	7		11	7
E10	20	17		17
G10	12	6	17	

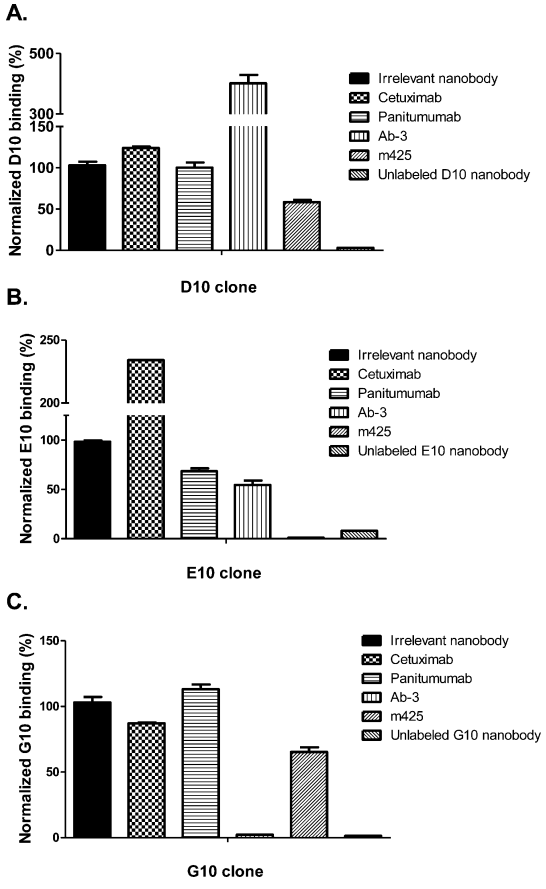

Figure 3. Competition between nanobodies and reference/therapeutic mAbs by flow cytometry. Panels A, B, and C represent the competition of d2-labeled nanobodies D10, E10, and G10, respectively. Cetuximab and panitumumab are both anti-ligand domain 3 binding site. m425 is the murine parental clone of matuzumab, binding domain III, outside the EFG binding region (this antibody acts like a negative allosteric modulator for ligand binding). Ab-3 (clone EGFR.1) binds EGFR domain I/II. Unlabeled nanobodies were used as positive competition control. Negative control was performed by adding an irrelevant nanobody (anti-ErbB2) as competitor. Labeled nanobodies and 50 μM mAb were incubated with 2×10^5 A431 cells for 2 h at 4 °C before washing and detection. Standard deviations represent two different experiments performed in triplicate.

nanobodies-d2 did compete with themselves (as unlabeled nanobodies) but did not compete with the two other nanobodies, demonstrating that three distinct EGFR epitopes are recognized by these three nanobodies. The apparent affinities of each nanobody were determined again in the presence of the other nanobodies (Table 2). Interestingly, the apparent affinity of G10-d2 for EGFR slightly increased in the presence of D10, but D10-d2 affinity was unaffected by the presence of G10.

TABLE 3. Affinity (K_d, nM) of Anti-EGFR Nanobodies in Competition with Different mAbs

	competitors				
clones	irrelevant nanobody	cetuximab	panitumumab	Ab-3	m425
D10	7	10	13	3	14
E10	20	11	70	67	*a*
G10	12	21	27	*a*	32

[a] No binding.

In an effort to localize more precisely these three different epitopes, we performed similar competition experiments using four well characterized anti-EGFR mAbs (cetuximab, panitumumab, Ab-3, and m425). Figure 3 shows results obtained by flow cytometry on A431 cells. D10 did not compete efficiently with any of these mAbs. Conversely, the binding of Ab-3 (antidomain I/II, clone EGFR.1[34]) strongly improved the binding of D10 (Table 3). E10 binding was totally abrogated in the presence of m425 (anti-domain III, murine parental clone of matuzumab[35]) but increased by a factor of 2 in the presence of cetuximab (targeting the ligand binding site on domain III[36]). These results suggest that E10 binds EGFR domain III away from the ligand binding site. Ab-3 efficiently competed with G10 suggesting that the epitope of this nanobody is located on domain I/II of EGFR. Finally, the presence of cetuximab and panitumumab did not hinder the binding of the three nanobodies suggesting that none of them is binding the EGFR ligand binding site.

EGFR Stimulation by Ligand Has a Major Effect on Nanobody Binding. Next, we investigated direct and indirect effects between ligand binding and nanobody binding. First, we checked whether the binding of nanobodies in the absence of ligand could have an influence on the phosphorylation of EGFR intracellular domain. Cells were incubated with saturating concentrations of nanobodies (1.5 μM for 10 min), and the phosphorylation status of EGFR was followed using an EGFR phosphorylation kit. Epidermal growth factor (EGF) and heregulin β (ErbB3 ligand) were used as a positive control and negative control, respectively. Figure 4A shows that under these conditions, and unlike EGF, nanobodies were not capable of directly triggering EGFR phosphorylation.

A direct effect on EGFR phosphorylation being excluded, we designed an HTRF competition experiment to determine whether the nanobodies could influence the ligand-induced phosphorylation (Figure 4B). Cetuximab, an anti-EGFR blocking antibody targeting the ligand binding site, was used as a

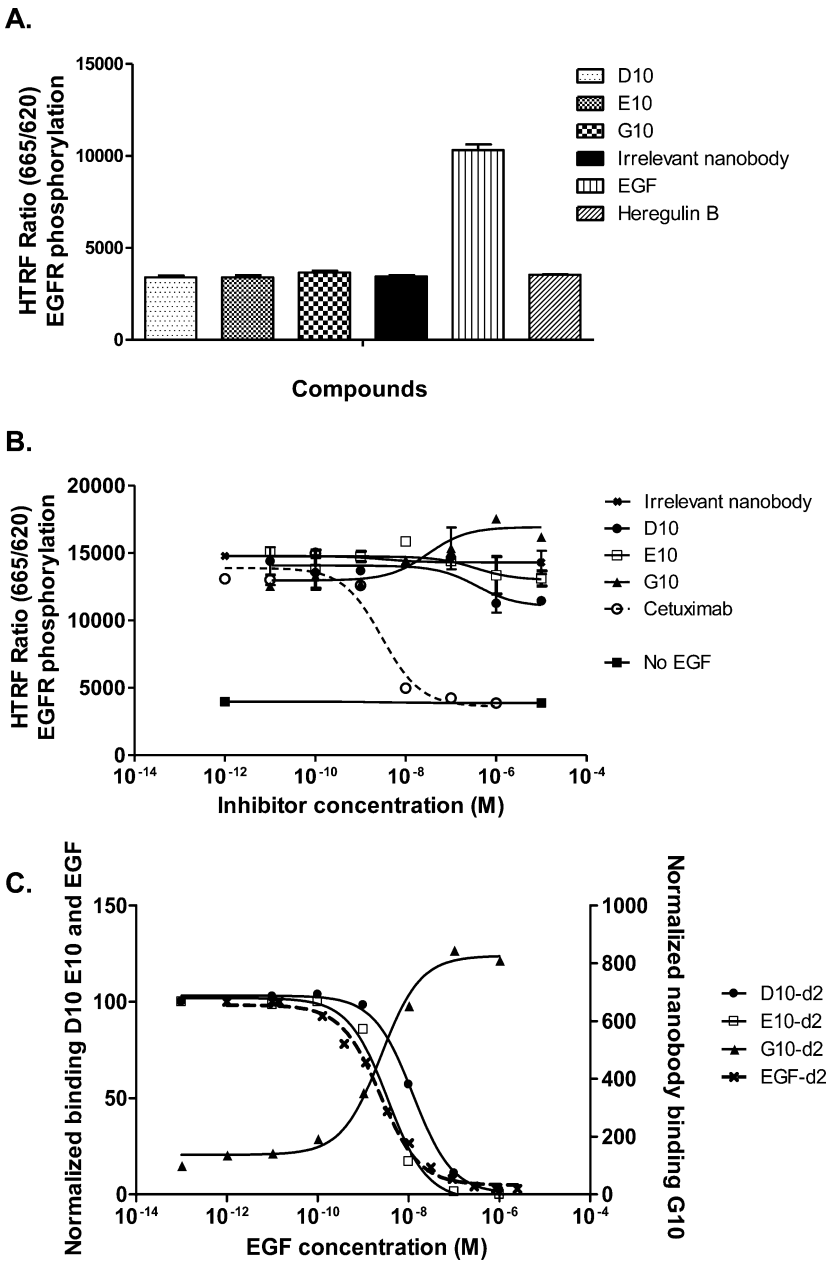

Figure 4. Competition with ligand and phosphorylation assays. (A) EGFR phosphorylation assays performed on A431 cells. Serum-free starved cells were stimulated by 1.5 μM ligand or nanobodies during 10 min at room temperature and were lysed. EGFR phosphorylation was detected using antibodies anti-EGFR-Tb (donor) and anti-phospho-d2 (acceptor). Energy transfer was measured after an overnight incubation. EGF was used to induce EGFR phosphorylation (positive control). Irrelevant nanobody (anti-ErbB3) and heregulin (ErbB3 ligand, does not bind EGFR) were used as negative controls. (B) Phosphorylation of EGFR stimulated by EGF (100 nM) in the presence or absence of different antibodies. Maximal phosphorylation was measured upon addition of an irrelevant nanobody (negative competition control). Cetuximab inhibits the EGFR phosphorylation by blocking the ligand binding site. (C) Competition of anti-EGFR nanobodies in the presence of EGF on A431 cells by flow cytometry. The graph was split in two parts, with a left *y*-axis corresponding to the normalized binding of D10-d2, E10-d2, and EGF-d2 and a right *y*-axis corresponding to normalized binding of G10-d2. EGF-d2 was used as a positive control for orthosteric competition.

positive control for inhibition. As expected, as low as 10 nM cetuximab could totally inhibit the EGF-induced phosphorylation by direct competition with EGF. In contrast, only a slight reduction of the EGFR phosphorylation (20%) could be measured using micromolar concentrations of D10 and E10. Interestingly, G10 led to a slight increase of EGF-induced phosphorylation efficiency, thereby acting as a weak positive allosteric modulator (PAM).

It is well-known that upon ligand binding, EGFR undergoes major conformational rearrangements. Thus, we investigated the influence of the presence of EGF on the binding efficiencies of anti-EGFR nanobodies by flow cytometry (Figure 4C). The presence of

EGF increased the affinity of G10 by a factor 8, suggesting that G10 preferentially binds the extended homodimer conformation of EGFR and clearly confirming that G10 does not bind to the EGFR ligand binding site. This result is also in line with its ability to act as a PAM by stabilizing the extended conformation of EGFR upon binding. Conversely, no binding of D10 and E10 to EGFR could be measured in the presence of an excess of ligand. An inverse correlation could be established between the EGF concentration and nanobody binding efficiency, similar to a direct competition between d2-labeled and unlabeled EGF performed as control (Figure 4C). Together with competition experiments using ligand binding site mAbs, these results suggest that D10 and E10, targeting two different epitopes, have an exquisite specificity for the tethered (inactive) conformation of EGFR and cannot bind to the extended conformation triggered by EGF binding.

D10, E10, and EGF Have Three Distinct Binding Sites. To strengthen this hypothesis and confirm that D10 and E10 do not directly compete for binding with EGF, we performed a Schild plot analysis by following EGFR phosphorylation in the presence of increasing concentrations of EGF and nanobodies (Figure 5A,B). By gradually increasing D10 concentrations, we could observe a gradual decrease in the maximal EGFR phosphorylation, but the half maximal effective concentration (EC_{50}) of EGF is weakly affected. In contrast, using E10 as competitor, we observed a roughly similar maximal phosphorylation and EC_{50} values increasing with the concentration of E10.

Despite these differences, the Schild plot analysis (Figure 5C) clearly demonstrated that both nanobodies behave as negative allosteric modulators (NAM). Indeed, slopes obtained using this analysis (0.17 and 0.45 for D10 and E10, respectively) are far from a slope equal to 1 that is expected for a competitive antagonist. Thus, these data confirm that E10 and D10 do not bind to the ligand binding site but instead behave as negative allosteric modulators by stabilizing the inactive (tethered) conformation of EGFR upon binding.

Nanobodies as EGFR Biosensors. EGFR binders with exquisite specificity for the tethered conformation (D10, E10) or with a strong preference for its extended form (G10) could be powerful tools to directly visualize the EGFR conformation on cells. To explore this possibility, we performed a model experiment using HEK293T cells transfected with EGFR-ST site-specifically labeled with a terbium donor fluorochrome. In this experiment, we followed the activation of EGFR due to the addition of EGF, followed by its subsequent inactivation due the addition of cetuximab, using our conformational probes labeled with an acceptor fluorochrome (d2) (Figure 6A). Controls were performed using an irrelevant nanobody coupled to d2 fluorochrome and heregulin as irrelevant ligand. A concentration of 100 nM of D10-d2 and E10-d2 were used to produce a high

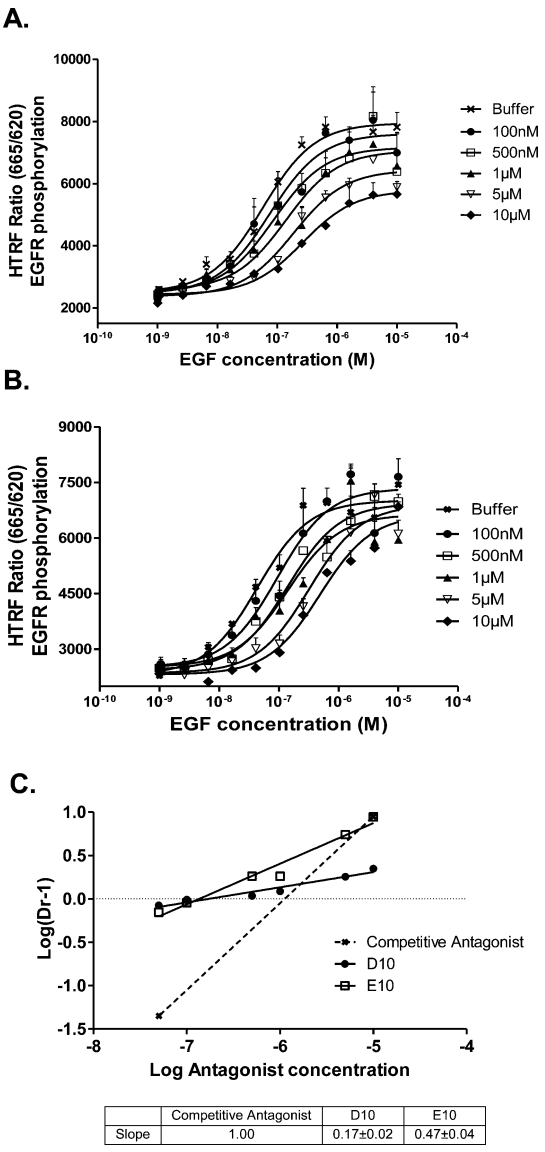

	Competitive Antagonist	D10	E10
Slope	1.00	0.17±0.02	0.47±0.04

Figure 5. Schild plot analysis. (A) Phosphorylation of EGFR on A431 cells, using various concentrations of EGF in the presence of five different concentrations of D10. EGFR phosphorylation was measured using the EGFR phosphorylation kit. (B) Phosphorylation of EGFR on A431 cells, using various concentrations of EGF in the presence of five different concentrations of E10. For panels A and B, A431 cells were starved in serum-free DMEM media 12 h before experiments were performed. (C) EGFR phosphorylation in the presence of D10 and E10. HTRF ratios were plotted as a regression of log (dose ratio − 1) versus log of molar concentrations of the antagonist (nanobodies). The slopes of resulting lines diverge from 1 (theoretical dotted line), indicating that both nanobodies are not competitive antagonists. The calculated slope values are 0.1745 (±0.02) and 0.4678 (±0.04) for D10 and E10, respectively. The theoretical curve corresponding to competitive and reversible antagonist is shown in dotted line in the graph. Standard deviations represent three different experiments performed in triplicate.

specific signal, while avoiding the NAM effect on EGF binding, negligible at this concentration (see Figure 4).

As expected, D10-d2 and E10-d2 binding yielded a high TR-FRET signal that decreased in a dose sensitive

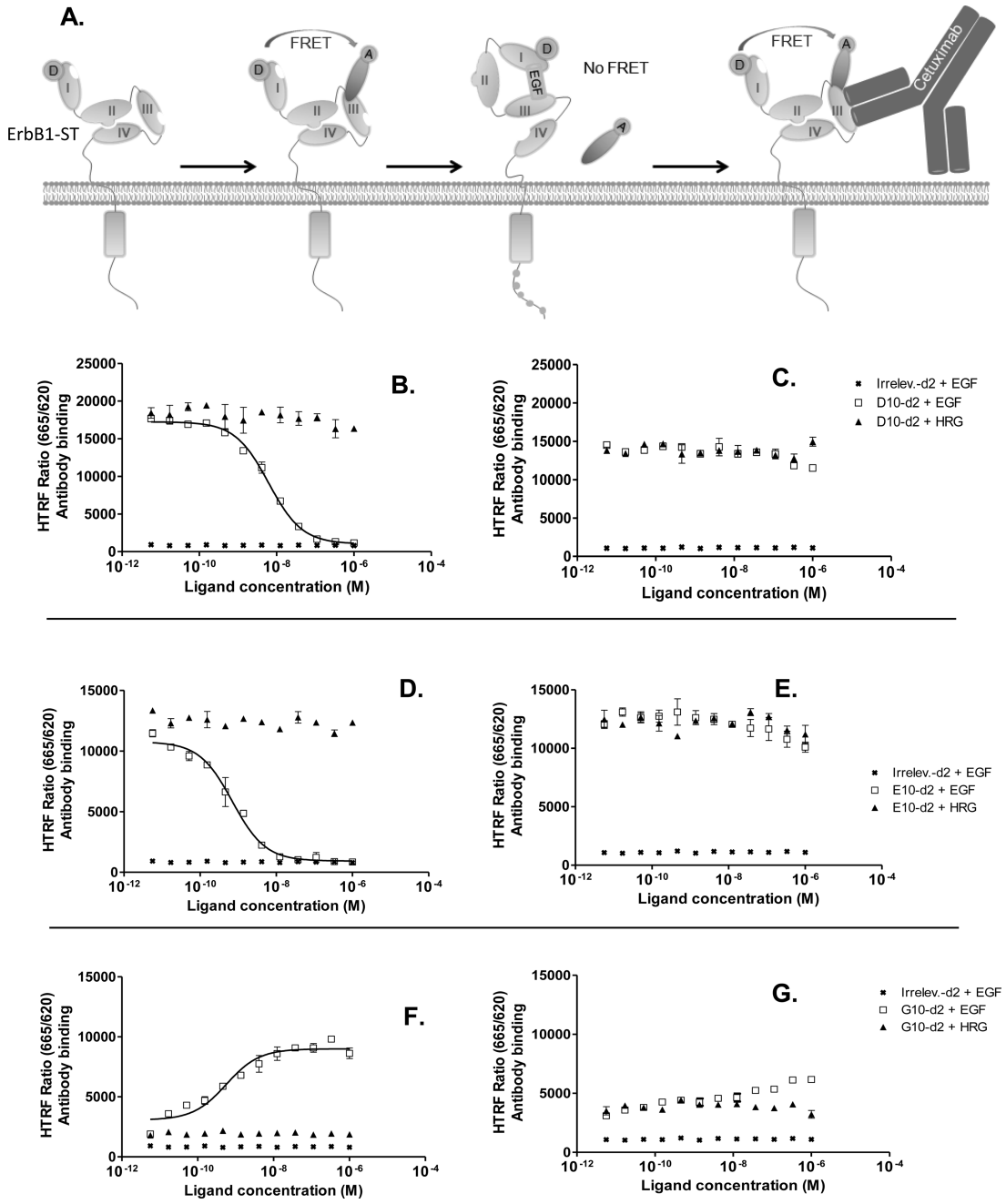

Figure 6. EGFR biosensor using anti-EGFR nanobodies by HTRF. (A) Cartoon representation of the biosensor experiments using energy transfer. EGFR-ST expressed on cells is covalently labeled with donor fluorochrome. A nanobody-d2 (acceptor) is added to cells, leading to energy transfer. Upon EGF ligand addition, EGFR is activated and a major conformational change occurs from tethered (inactivated) to an extended (activated) conformation, unfavorable to nanobody binding. After a subsequent addition of an excess of cetuximab blocking the ligand binding site, EGFR recovers its inactive conformation, allowing the rebinding of the nanobody-d2. For the sake of clarity, only one protomer is represented here. (B) Binding of D10-d2 (100 nM) or irrelevant-d2 clone (anti-ErbB2, 100 nM) on EGFR-ST-Tb (donor-labeled receptor), in the presence of increasing concentration of ligands. Irrelevant nanobody-d2 and heregulin (HRG) were used as a negative controls. TR-FRET signals were measured for panels B, D, and F after 1 h of incubation with ligand at 4 °C. Subsequently, a 1 μM final concentration of cetuximab was added in wells, and TR-FRET signals were measured for panels C, E, and G after 2 h incubation. Experiments were performed with 100 nM D10-d2 (B, C), 100 nM E10-d2 (D, E), and 20 nM G10-d2 (F, G).

fashion upon addition of EGF, thereby directly visualizing the EGFR conformational change (Figure 6B,D). Strikingly, the addition of cetuximab to the mixture could fully restore the TR-FRET signal by competing out the ligand, thereby switching EGFR to its original tethered conformation (Figure 6C,E). Conversely, G10-d2 used at low concentrations (20 nM) yielded a faint signal in the absence of EGF, which increased in a dose dependent fashion upon addition of EGF, visualizing the appearance of the extended/homodimeric form of EGFR (Figure 6F). As in the previous experiment, the subsequent addition of cetuximab

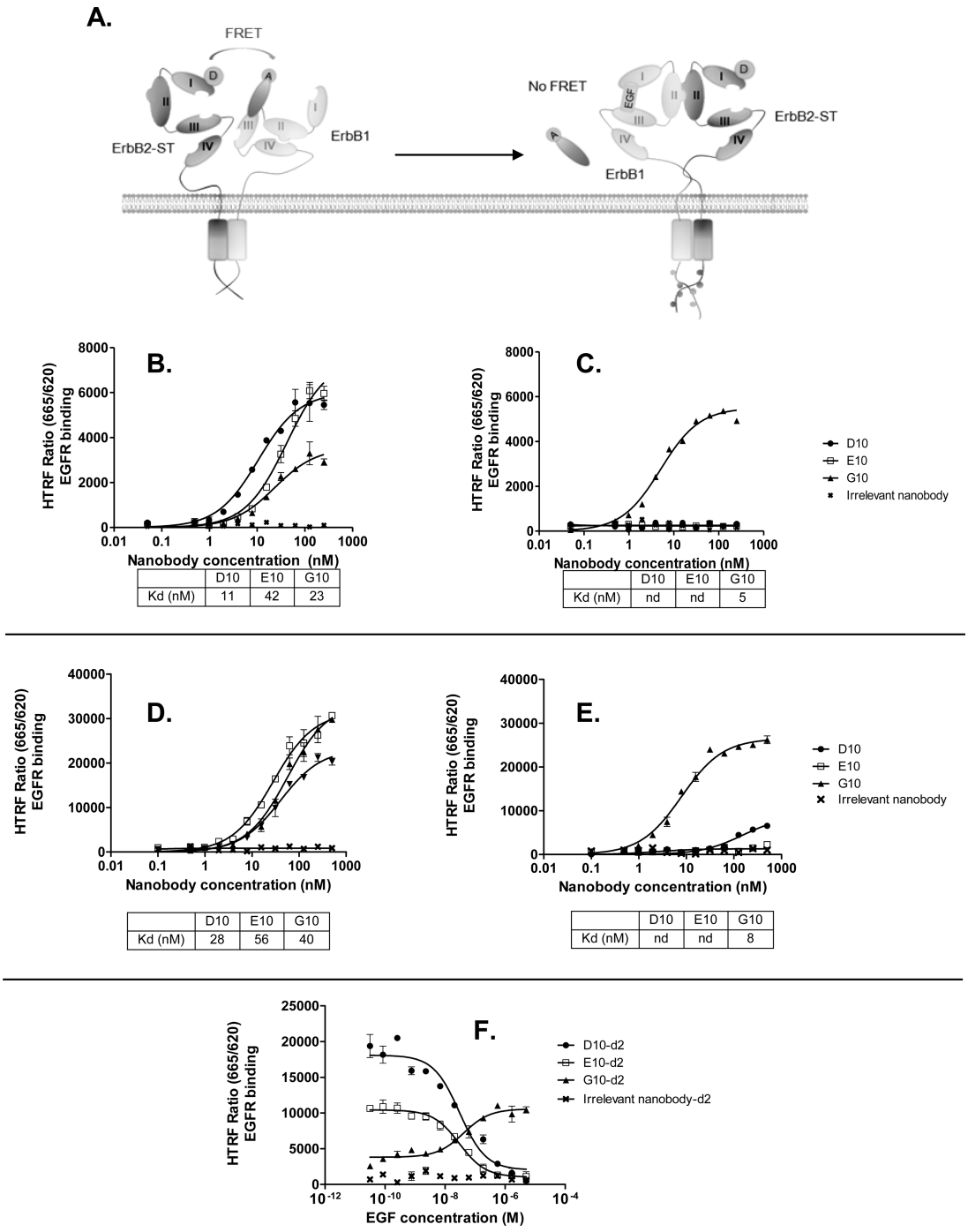

	D10	E10	G10
Kd (nM)	11	42	23

	D10	E10	G10
Kd (nM)	nd	nd	5

	D10	E10	G10
Kd (nM)	28	56	40

	D10	E10	G10
Kd (nM)	nd	nd	8

Figure 7. Conformational biosensors reveal tethered EGFR involved in EGFR/ErbB2 predimers. (A) Cartoon depicting the use of anti-EGFR nanobodies as biosensors on EGFR/ErbB2 predimers. TR-FRET can be measured between donor-labeled ErbB2-ST receptor and d2-labeled nanobody. (B) Affinity of D10, E10, and G10 on EGFR/ErbB2 heterodimers. HEK293T cells were transfected with wild-type ErbB1 and ErbB2-ST. Donor fluorochrome was covalently labeled on ErbB2 receptor. Nanobodies were added at various concentrations and were detected using 200 nM anti-6His-d2, leading to a TR-FRET signal restricted to heterodimers. (C) Anti-EGFR nanobodies affinity on EGFR/ErbB2 heterodimers in the presence of 500 nM EGF. (D, E) Affinity of nanobodies D10, E10, and G10 on NIH/3T3 cells cotransfected with wild-type ErbB2 and wild-type EGFR. A donor fluorochrome was coupled to an anti-ErbB2 mAb. The TR-FRET signal was measured after 2 h of incubation at 4 °C with (E) or without (D) 500 nM EGF. (F) EGFR conformational rearrangement followed by d2-labeled nanobodies on wild-type EGFR/ErbB2 heterodimers on NIH/3T3 transfected cells in the presence of increasing concentrations of EGF. The energy transfer between donor labeled anti-ErbB2 mAb and d2-labeled nanobodies was used to monitor the EGF-induced conformational change of EGFR. Experiments were performed with 100 nM D10-d2, 100 nM E10-d2, and 20 nM G10-d2.

re-established the tethered EGFR conformation, thereby drastically reducing the TR-FRET signal (Figure 6G). Altogether, these results demonstrated that these anti-EGFR nanobodies could be used as sensors of "activated/extended" and "inactivated/tethered" conformation of EGFR.

Conformational Biosensors Reveal Tethered EGFR Involved in EGFR/ErbB2 Predimers. We finally took advantage of these innovative tools to study the conformation of EGFR involved in the heterodimer EGFR/ErbB2, in the presence or absence of ligand.

For this purpose, we followed the transfer of fluorescence between the donor fluorochrome on ErbB2 receptor (*via* a ST fusion or an anti-ErbB2-Tb mAb) and nanobodies bound to a wild-type EGFR revealed by anti-6His-d2 or directly labeled. In these conditions, a TR-FRET signal can only be generated by EGFR/ErbB2 heterodimers as shown in Figure 7A. Strikingly, a strong signal was measured using the three nanobodies in the absence of EGF (Figure 7B). As expected, upon addition of EGF, the signal obtained using the "tethered conformation" specific nanobodies D10 and E10 was totally abrogated, due to the EGF-induced EGFR conformational change (Figure 7C). In these conditions, the presence of EGFR/ErbB2 dimers could still be monitored since, in contrast to D10 and E10, G10 yielded a much stronger signal owing to its higher affinity for extended EGFR.

To fully establish the biological relevance of this finding, we explored the possibility to detect tethered EGFR engaged in predimers using wild-type ErbB receptors. The murine nonblocking donor-labeled mAb (FRP5) was used to target ErbB2. As shown in Figure 7D,E, very similar results were obtained, demonstrating that wild-type ErbB receptors efficiently form EGFR/ErbB2 heterodimers in the absence of ligand while predominantly adopting a tethered conformation. Interestingly, the proportion of tethered and extended EGFR varied according to the concentration of EGF (Figure 7F), thereby reproducing the results obtained with EGFR expressed in the absence of ErbB2.

Altogether, these experiments confirm that EGFR can form heterodimers with ErbB2 in the absence of ligand and directly demonstrate that within these predimers, EGFR adopts a tethered/inactive conformation despite its stable interaction with ErbB2. These results also confirm that EGFR engaged in predimers switch to the extended/active conformation in the presence of ligand.

DISCUSSION

In this study, using phage display we selected nanobodies against the epidermal growth factor receptor from the repertoire of an immunized llama. Three EGFR specific clones, with no cross reaction with other members of the ErbB family, were fully characterized. Nanobodies D10, E10, and G10 bind three distinct epitopes of their target with a high affinity (7, 20, and 12 nM, respectively). Competition experiments with reference mAbs cetuximab,[37] panitumumab,[37] Ab-3,[34] and m425[38] demonstrated that none of these nanobodies target the ligand binding site despite the fact that two of these nanobodies cannot bind EGFR in the presence of its ligand. Instead, nanobodies D10 and E10 bind EGFR epitopes that are only present in the inactive conformation of this receptor known to undergo major conformational changes upon ligand binding.[7,39,40] In contrast G10 binds both conformations of the receptor, but with an 8-fold higher apparent affinity for the active conformation. These results highlight the caution that should be taken when interpreting the results of competition experiments of two binders. Indeed, the stabilization of an alternative conformation of their target can be misinterpreted as a direct steric hindrance effect due to the targeting of a common epitope. Interestingly, despite their strong binding to a specific conformation of EGFR, these nanobodies only lead to weak positive (G10) or negative (D10, E10) allosteric modulation of EGF-driven EGFR phosphorylation, qualifying them as sensitive conformational sensors. This is in contrast to previously selected EGFR specific nanobodies inducing strong orthosteric or allosteric modulations.[41,42]

Previous data have demonstrated the presence of EGFR predimers on resting cells,[20,43,44] estimated to represent about 40% of the total population of EGFRs.[45] Some studies have suggested that ligand-independent EGFR predimerization is a mechanism allowing the induction of a faster signal transduction when receptors are stimulated with ligand.[46,47] Teramura et al. suggested that monomers of EGFR exist primarily in the tethered state and that the formation of predimers biases the structure of EGFR toward extended state-like conformations with high association rates to EGF,[46] inducing a dynamic conformational change in the predimer that facilitates and accelerates the formation of signaling dimer of EGF/EGFR complexes. Authors argue that large increases in the association rate of EGF to the predimer binding sites suggest that the conformation resembles the extended form. The association of EGF with one of the EGFR molecules in the dimer sites might trigger an allosteric conformational change in the EGF binding site in the other EGFR molecule, which could explain a positive cooperativity upon EGF binding. This concept is also favored by molecular dynamic simulations performed by Arkhipov et al.[21] These authors performed molecular dynamics on the crystal structure of the two-ligand extracellular dimer after removal of the EGF and obtained an "active-like" conformation, except for domain IV showing a bending motion that would favor the formation of symmetric (inactive) kinase dimers.[16]

CONCLUSION

In this paper, we demonstrate that in the absence of ligand, EGFR is also engaged in dimers with ErbB2 as preheterodimers. However, unlike the situation described above with EGFR prehomodimers, EGFR displays a conformation very similar to the tethered

inactive conformation. Upon EGF stimulation, EGFR adopts the extended conformation allowing the signaling to occur. While the significance of these discrepancies deserves further studies, this finding has importance for the design of efficient inhibitors. Indeed, ErbB2 is frequently overexpressed in a variety of cancers and has a strong capacity to form heterodimers with ErbB3 and EGFR and with ErbB4 to a lesser extent.[48] In such situations, a very significant part of EGFR is thought to be engaged in EGFR/ErbB2 predimers. Our results imply that the most efficient inhibitors should thus be designed to interact with the tethered conformation of EGFR. Finally, while the anti-EGFR nanobodies described in this work have an intrinsic value as conformational sensors, they might also be advantageously used for other applications, including imaging, targeting, or high throughput screening approaches aimed at identifying new EGFR inhibitors targeting the extracellular portion of the receptor.

MATERIALS AND METHODS

Reagents, Cell Lines, and Antibodies. HEK293T, NIH/3T3, and A431 cells were obtained from ATCC. Cells lines were cultivated in DMEM (Invitrogen) complemented with 10% (v/v) Bovine Serum gold (PAA). Cetuximab and panitumumab were a kind gift of Rémi Castellano (CRCM U1068). All HTRF reagents, labeled antibodies, labeled ligands, and SNAP-tag plasmids were a kind gift from Cisbio Bioassays.

Llama Immunization and Library Construction. A llama (*Lama glama*) was immunized subcutaneously 4 times at 15 days intervals with 100 μg of recombinant human EGFR/Fc chimera (344ER, R&D Systems), using a previously published protocol,[49,50] and VHH library construction was performed in *Escherichia coli* TG1 strain as previously described.[49,50] Library diversities were above 10^8 transformants.

Selection of Nanobodies by Phage Display. Twenty microliters of the bacteria library was grown in 50 mL of 2YTAG (2YT/ampicillin (100 μg/mL)/2% glucose) at 37 °C with shaking (250 rpm) to an OD_{600} between 0.5 and 0.7. Bacteria were infected by KM13 helper phage using a multiplicity of infection of 20, during 30 min at 37 °C without shaking. The culture was centrifuged for 15 min at 3000*g*, and the bacterial pellet was resuspended in 250 mL of 2YTA/kanamycin (50 μg/mL) overnight at 30 °C with shaking. The overnight culture was split in 10 vials and centrifuged for 20 min at 3000*g*. Five milliliters of 80% PEG8000/2.5 mM NaCl was added to the supernatant in a new clean vial and incubated for 1 h on ice. The solution was centrifuged for 20 min at 3000*g* at 4 °C, and the phage-containing pellet was resuspended in 1 mL of PBS. Another centrifugation step (2 min, 14000*g*) was performed to eliminate bacterial contaminant, and 200 μL of PEG8000/NaCl was added to supernatants in a new vial. After 30 min on ice and a last centrifugation (5 min, 14000*g*), phage-containing pellets were resuspended in 1 mL of PBS. To obtain EGFR specific clones, a first round of selection was performed on magnetic Epoxybeads (Dynabeads, Invitrogen) coupled to EGFR-Fc during 48 h at 4 °C following recommendations of the manufacturer. Before selection on EGFR-Fc/Epoxybeads, the phage−nanobody library was depleted by incubation with ErbB2-Fc/Epoxybeads to eliminate anti-Fc and anti-ErbB2 antibodies and to reduce nonspecific binding. Remaining phages and EGFR-coated beads were saturated with 2% milk/PBS during 1 h at 4 °C. Next, phages and EGFR-Fc/Epoxybeads were incubated together during 2 h at 4 °C with shaking. Beads were washed 5 times with 1 mL of 0.1% Tween PBS and 5 times with PBS. Bound phages were eluted using 1 mg/mL trypsin solution (Sigma) during 30 min at room temperature with shaking. Phages were rescued and amplified by infection of *E. coli* TG1 strain and phage production as above, yielding S1 polyclonal phage population.

To avoid selection against the Fc domain and to select antibodies against wild-type EGFR, a second round of selection (S2) was performed on the A431 cell line (2×10^7 cells), which expresses a large amount of EGFR. The S1 polyclonal phage population and cells were saturated in 2% milk/PBS during 1 h at 4 °C and incubated together in same conditions described previously. After five PBS washes, bound phages were eluted using trypsin solution (1 mg/mL) during 30 min at room temperature. Phages were rescued in *E. coli* TG1, and infected bacteria corresponding to S2 were plated. Individual *E. coli* TG1 colonies from S2 were picked and grown in two different 96-deep-well plates in 400 μL of 2YTAG. After overnight growth, half of the culture was frozen at −80 °C in 20% glycerol for backup, and the rest of culture was used for soluble nanobody production induced by isopropyl-β-D-thio galactopyranoside (IPTG). Nanobody concentrations in supernatant were estimated at 100−500 nM using the Double-Tag check kit (Cisbio Bioassays).

Production and Purification of Nanobodies. For large scale nanobody production, positive phagemids from the screening step were transformed in *E. coli* BL21DE3 strain. Transformed bacteria were grown in 400 mL of 2YTA until OD_{600}= 0.7 and induced with 100 μM IPTG for an overnight growth at 30 °C with shaking. Bacteria were pelleted and lysed by freeze−thawing and Bugbuster Protein Extraction Reagent (Novagen). After a centrifugation step (3000*g*, 20 min), nanobodies were purified from the supernatant using metal affinity chromatography, TALON Superflow (GE Healthcare), according to the manufacturer's instructions.[51]

Fluorochrome Labeling of Nanobodies. Purified nanobodies were dialyzed during 24 h against a 50 mM phosphate buffer, pH 8, with a 10 kDa cutoff membrane. After dialysis, fluorochrome (Tb-NHS and d2-NHS) and nanobodies were added using a 6:1 molarity ratio during 45 min at room temperature with shaking. After incubation, labeled nanobodies were separated by gel filtration chromatography (NAP5/10/25, GE Healthcare) according to protein quantity. Chromatography columns were equilibrated with 100 mM phosphate buffer, pH 7, before loading proteins. Purified samples were eluted from the column with phosphate buffer and split into 100 μL fractions. For each fraction, a wavelength scan measurement was performed to calculate fluorochrome/nanobodies ratio. Fractions with similar relative median fluorescence (2, 2.1, and 2.5 for D10-d2, E10-d2, and G10-d2, respectively) were pooled.

Flow Cytometry Experiments. All flow cytometry experiments were performed at 4 °C and in 96 well plates using 2×10^5 cells/well. Cells were saturated by PBS/2% BSA solution during 1 h with shaking to avoid nonspecific binding. For screening, 75 μL of nanobody-containing supernatant was added to 75 μL of cells in PBS/2% BSA and incubated for 1 h. After three washes in PBS/2% BSA, cells were incubated for 1 h with a 1/500 dilution of anti-6His tag antibody (Novagen), washed 3 times with PBS/2% BSA, and incubated for 1 h with a 1/200 dilution of PE-conjugated goat anti-mouse antibody (SantaCruz). After three last washes in PBS, fluorescence was measured using a MACSQuant cytometer (Miltenyi), and results were analyzed with the MACSQuant software.

For binding and competition experiments on purified fluorochrome-labeled nanobodies, 75 μL of 2% BSA/PBS containing 100 μM competitors (therapeutic mAbs, nanobodies, or ligands) was added to cells followed by 75 μL of purified labeled nanobodies at 50, 190, and 160 nM for D10-d2, E10-d2, and G10-d2, respectively. After 2 h at 4 °C with shaking, cells were washed 3 times in PBS, and mean fluorescence intensity (MFI) was measured on cytometer for each sample.

Homogenous Time Resolved Fluorescence (HTRF) Assays. All HTRF[52] experiments were performed on white 384sv well plates

(Corning) and read on TECAN Infinite M1000. ErbB-SNAP-Tag plasmids (ErbB-ST, Cisbio bioassays) were FLAG tagged, and the ErbB4-HaloTag construction (ErbB4-HT, Cisbio bioassays) was c-myc tagged. SNAP-Tag-fused ErbB family receptors are totally active and present the same pharmacology as wild-type receptors (Validated by Cisbio Bioassays). Binding assays were performed using HEK293T cells transfected with ErbB-ST and HT receptors. After a 24 h transfection using Lipofectamine 2000 (Invitrogen) following the constructor's recommendation, adherent cells were washed with prewarmed Tag-lite buffer. Cells were incubated with 100 nM Lumi4-Tb (Donor fluorochrome coupled on specific substrate from Cisbio Biossays) for 1 h at 37 °C. During this step, terbium cryptate fluorochrome was covalently coupled to ErbB receptors via the SNAP-Tag fusion. Cells were washed 4 times directly on flasks using Tag-lite buffer and were detached from their support using Accutase solution (Thermo). After two final Tag-lite washes, 10 μL of ErbB-ST-Tb cells were dispensed on small volume wells with 5000 or 10000 cells/well. Nanobodies were incubated with transfected cells and revealed generally by 200 nM anti-6His-d2. When labeled nanobodies-d2 were used, anti-6His-d2 was replaced by 5 μL of Tag-lite buffer. After 2 h incubation at 4 °C, d2 acceptor TR-FRET signal (665 nm) and Tb donor signal (620 nm) were measured using a 60 μs delay and a 400 μs integration upon excitation at 337 nm (on TECAN Infinite M1000). HTRF ratio (665 nm/620 nm $\times$ 10^4) was calculated to prevent interference due to medium variability or chemical compound or to normalize experiments when cells expressing different receptor levels were used.[52] For competition experiments, competitors were incubated with nanobodies, and fluorescence was measured after waiting for equilibrium (usually 2 h at 4 °C). EGFR phosphorylation assays were performed using the Phospho-EGFR (Tyr1068) cellular assay kit (Cisbio Bioassays) following the manufacturer's recommendations. Data from HTRF experiments were analyzed using GraphPad Prism.

Enzyme Linked Immunosorbent Assay (ELISA). ErbB1-Fc, ErbB2-Fc, ErbB3-Fc, and ErbB4-Fc chimera proteins (R&D Systems), 100 μL at 10 μg/mL, were incubated in each well on Maxisorp plate (Nunc) during 24 h at 4 °C. After protein absorption, wells were saturated with PBS/2% BSA for 1 h at room temperature and incubated with 50 μL of purified nanobodies (2 μg/mL) during 1 h at 4 °C with shaking. Nonbound nanobodies were washed 3 times in PBS/2%BSA. Nanobodies were detected using 50 μL of a 1/1000 dilution of anti-6His antibody (Novagen), washed 3 times with PBS/2% BSA, and incubated for 1 h with a 1/5000 dilution of HRP-conjugated goat anti-mouse antibody (Jackson Immunoresearch lab). After 1 h incubation and three washes with 0.1% Tween PBS followed by three washes in PBS, bound secondary antibodies were detected using ABTS (2 2′-azinobis(3-ethylbenzthiazoline-6-sulfonic acid), Sigma). Absorbance was measured at 405 nm on TECAN Infinite M1000.

Conflict of Interest: The authors declare no competing financial interest.

Acknowledgment. This work was supported by a national FUI Project (Cell2Lead). We thank Cisbio Biassays and particularly Hervé Bazin for all compounds, SNAP-tagged receptors, and reagents, as well as all ATI team (CRCM) for help and support. D.N. performed most experiments, B.L. performed some experiments, D.N., D.B., and P.C. designed the experiments, D.N., D.B., and P.C. wrote the manuscript. E.D. designed and followed SNAP-tag and HALOTag reagents and experiments. G.M. initiated the project and supervised it together with D.B. and P.C.

Supporting Information Available: Amino acid sequences of the complementarity determining regions of selected nanobodies. This material is available free of charge *via* the Internet at http://pubs.acs.org.

REFERENCES AND NOTES

1. Oda, K.; Matsuoka, Y.; Funahashi, A.; Kitano, H. A Comprehensive Pathway Map of Epidermal Growth Factor Receptor Signaling. *Mol. Syst. Biol.* **2005**, *1* (2005), No. 0010.
2. Roskoski, R., Jr. The Erbb/Her Family of Protein-Tyrosine Kinases and Cancer. *Pharmacol. Res.* **2014**, *79*, 34–74.
3. Lemmon, M. A. Ligand-Induced Erbb Receptor Dimerization. *Exp. Cell Res.* **2009**, *315*, 638–648.
4. Cho, H. S.; Leahy, D. J. Structure of the Extracellular Region of Her3 Reveals an Interdomain Tether. *Science* **2002**, *297*, 1330–1333.
5. Ferguson, K. M.; Berger, M. B.; Mendrola, J. M.; Cho, H. S.; Leahy, D. J.; Lemmon, M. A. Egf Activates Its Receptor by Removing Interactions That Autoinhibit Ectodomain Dimerization. *Mol. Cell* **2003**, *11*, 507–517.
6. Garrett, T. P.; McKern, N. M.; Lou, M.; Elleman, T. C.; Adams, T. E.; Lovrecz, G. O.; Zhu, H. J.; Walker, F.; Frenkel, M. J.; Hoyne, P. A.; et al. Crystal Structure of a Truncated Epidermal Growth Factor Receptor Extracellular Domain Bound to Transforming Growth Factor Alpha. *Cell* **2002**, *110*, 763–773.
7. Ogiso, H.; Ishitani, R.; Nureki, O.; Fukai, S.; Yamanaka, M.; Kim, J. H.; Saito, K.; Sakamoto, A.; Inoue, M.; Shirouzu, M.; et al. Crystal Structure of the Complex of Human Epidermal Growth Factor and Receptor Extracellular Domains. *Cell* **2002**, *110*, 775–787.
8. Schlessinger, J. Ligand-Induced, Receptor-Mediated Dimerization and Activation of Egf Receptor. *Cell* **2002**, *110*, 669–672.
9. Zhang, X.; Gureasko, J.; Shen, K.; Cole, P. A.; Kuriyan, J. An Allosteric Mechanism for Activation of the Kinase Domain of Epidermal Growth Factor Receptor. *Cell* **2006**, *125*, 1137–1149.
10. Moriki, T.; Maruyama, H.; Maruyama, I. N. Activation of Preformed Egf Receptor Dimers by Ligand-Induced Rotation of the Transmembrane Domain. *J. Mol. Biol.* **2001**, *311*, 1011–1026.
11. Junttila, T. T.; Akita, R. W.; Parsons, K.; Fields, C.; Lewis Phillips, G. D.; Friedman, L. S.; Sampath, D.; Sliwkowski, M. X. Ligand-Independent Her2/Her3/Pi3k Complex Is Disrupted by Trastuzumab and Is Effectively Inhibited by the Pi3k Inhibitor Gdc-0941. *Cancer Cell* **2009**, *15*, 429–440.
12. Kawashima, N.; Nakayama, K.; Itoh, K.; Itoh, T.; Ishikawa, M.; Biju, V. Reversible Dimerization of Egfr Revealed by Single-Molecule Fluorescence Imaging Using Quantum Dots. *Chemistry* **2010**, *16*, 1186–1192.
13. Gadella, T. W., Jr.; Jovin, T. M. Oligomerization of Epidermal Growth Factor Receptors on A431 Cells Studied by Time-Resolved Fluorescence Imaging Microscopy. A Stereochemical Model for Tyrosine Kinase Receptor Activation. *J. Cell Biol.* **1995**, *129*, 1543–1558.
14. Yu, X.; Sharma, K. D.; Takahashi, T.; Iwamoto, R.; Mekada, E. Ligand-Independent Dimer Formation of Epidermal Growth Factor Receptor (Egfr) Is a Step Separable from Ligand-Induced Egfr Signaling. *Mol. Biol. Cell* **2002**, *13*, 2547–2557.
15. Macdonald-Obermann, J. L.; Piwnica-Worms, D.; Pike, L. J. Mechanics of Egf Receptor/Erbb2 Kinase Activation Revealed by Luciferase Fragment Complementation Imaging. *Proc. Natl. Acad. Sci. U. S. A.* **2012**, *109*, 137–142.
16. Jura, N.; Endres, N. F.; Engel, K.; Deindl, S.; Das, R.; Lamers, M. H.; Wemmer, D. E.; Zhang, X.; Kuriyan, J. Mechanism for Activation of the Egf Receptor Catalytic Domain by the Juxtamembrane Segment. *Cell* **2009**, *137*, 1293–1307.
17. Endres, N. F.; Das, R.; Smith, A. W.; Arkhipov, A.; Kovacs, E.; Huang, Y.; Pelton, J. G.; Shan, Y.; Shaw, D. E.; Wemmer, D. E.; et al. Conformational Coupling across the Plasma Membrane in Activation of the Egf Receptor. *Cell* **2013**, *152*, 543–556.
18. Mi, L. Z.; Lu, C.; Li, Z.; Nishida, N.; Walz, T.; Springer, T. A. Simultaneous Visualization of the Extracellular and Cytoplasmic Domains of the Epidermal Growth Factor Receptor. *Nat. Struct. Mol. Biol.* **2011**, *18*, 984–989.
19. Liu, P.; Cleveland, T. E., IV; Bouyain, S.; Byrne, P. O.; Longo, P. A.; Leahy, D. J. A Single Ligand Is Sufficient to Activate EGFR Dimers. *Proc. Natl. Acad. Sci. U. S. A.* **2012**, *109*, 10861–10866.
20. Macdonald-Obermann, J. L.; Adak, S.; Landgraf, R.; Piwnica-Worms, D.; Pike, L. J. Dynamic Analysis of the Epidermal

Growth Factor (Egf) Receptor-Erbb2-Erbb3 Protein Network by Luciferase Fragment Complementation Imaging. *J. Biol. Chem.* **2013**, *288*, 30773–30784.
21. Arkhipov, A.; Shan, Y.; Das, R.; Endres, N. F.; Eastwood, M. P.; Wemmer, D. E.; Kuriyan, J.; Shaw, D. E. Architecture and Membrane Interactions of the Egf Receptor. *Cell* **2013**, *152*, 557–569.
22. Muyldermans, S. Nanobodies: Natural Single-Domain Antibodies. *Annu. Rev. Biochem.* **2013**, *82*, 775–797.
23. Perez, J. M.; Renisio, J. G.; Prompers, J. J.; van Platerink, C. J.; Cambillau, C.; Darbon, H.; Frenken, L. G. Thermal Unfolding of a Llama Antibody Fragment: A Two-State Reversible Process. *Biochemistry* **2001**, *40*, 74–83.
24. Gueorguieva, D.; Li, S.; Walsh, N.; Mukerji, A.; Tanha, J.; Pandey, S. Identification of Single-Domain, Bax-Specific Intrabodies That Confer Resistance to Mammalian Cells against Oxidative-Stress-Induced Apoptosis. *FASEB J.* **2006**, *20*, 2636–2638.
25. Muyldermans, S. Single Domain Camel Antibodies: Current Status. *J. Biotechnol.* **2001**, *74*, 277–302.
26. De Genst, E.; Silence, K.; Decanniere, K.; Conrath, K.; Loris, R.; Kinne, J.; Muyldermans, S.; Wyns, L. Molecular Basis for the Preferential Cleft Recognition by Dromedary Heavy-Chain Antibodies. *Proc. Natl. Acad. Sci. U. S. A.* **2006**, *103*, 4586–4591.
27. Irannejad, R.; Tomshine, J. C.; Tomshine, J. R.; Chevalier, M.; Mahoney, J. P.; Steyaert, J.; Rasmussen, S. G.; Sunahara, R. K.; El-Samad, H.; Huang, B.; et al. Conformational Biosensors Reveal Gpcr Signalling from Endosomes. *Nature* **2013**, *495*, 534–538.
28. Staus, D. P.; Wingler, L. M.; Strachan, R. T.; Rasmussen, S. G.; Pardon, E.; Ahn, S.; Steyaert, J.; Kobilka, B. K.; Lefkowitz, R. J. Regulation of Beta2-Adrenergic Receptor Function by Conformationally Selective Single-Domain Intrabodies. *Mol. Pharmacol.* **2014**, *85*, 472–481.
29. Ho-Pun-Cheung, A.; Bazin, H.; Gaborit, N.; Larbouret, C.; Garnero, P.; Assenat, E.; Castan, F.; Bascoul-Mollevi, C.; Ramos, J.; Ychou, M.; et al. Quantification of Her Expression and Dimerization in Patients' Tumor Samples Using Time-Resolved Forster Resonance Energy Transfer. *PLoS One* **2012**, *7*, No. e37065.
30. Mathis, G. Probing Molecular Interactions with Homogeneous Techniques Based on Rare Earth Cryptates and Fluorescence Energy Transfer. *Clin Chem.* **1995**, *41*, 1391–1397.
31. Juillerat, A.; Gronemeyer, T.; Keppler, A.; Gendreizig, S.; Pick, H.; Vogel, H.; Johnsson, K. Directed Evolution of O6-Alkylguanine-DNA Alkyltransferase for Efficient Labeling of Fusion Proteins with Small Molecules in Vivo. *Chem. Biol.* **2003**, *10*, 313–317.
32. Gautier, A.; Juillerat, A.; Heinis, C.; Correa, I. R., Jr.; Kindermann, M.; Beaufils, F.; Johnsson, K. An Engineered Protein Tag for Multiprotein Labeling in Living Cells. *Chem. Biol.* **2008**, *15*, 128–136.
33. Maurel, D.; Comps-Agrar, L.; Brock, C.; Rives, M. L.; Bourrier, E.; Ayoub, M. A.; Bazin, H.; Tinel, N.; Durroux, T.; Prezeau, L.; et al. Cell-Surface Protein-Protein Interaction Analysis with Time-Resolved Fret and Snap-Tag Technologies: Application to Gpcr Oligomerization. *Nat. Methods* **2008**, *5*, 561–567.
34. Cochran, J. R.; Kim, Y. S.; Olsen, M. J.; Bhandari, R.; Wittrup, K. D. Domain-Level Antibody Epitope Mapping through Yeast Surface Display of Epidermal Growth Factor Receptor Fragments. *J. Immunol. Methods* **2004**, *287*, 147–158.
35. Rodeck, U.; Herlyn, M.; Herlyn, D.; Molthoff, C.; Atkinson, B.; Varello, M.; Steplewski, Z.; Koprowski, H. Tumor Growth Modulation by a Monoclonal Antibody to the Epidermal Growth Factor Receptor: Immunologically Mediated and Effector Cell-Independent Effects. *Cancer Res.* **1987**, *47*, 3692–3696.
36. Li, S.; Schmitz, K. R.; Jeffrey, P. D.; Wiltzius, J. J.; Kussie, P.; Ferguson, K. M. Structural Basis for Inhibition of the Epidermal Growth Factor Receptor by Cetuximab. *Cancer Cell* **2005**, *7*, 301–311.
37. Voigt, M.; Braig, F.; Gothel, M.; Schulte, A.; Lamszus, K.; Bokemeyer, C.; Binder, M. Functional Dissection of the Epidermal Growth Factor Receptor Epitopes Targeted by Panitumumab and Cetuximab. *Neoplasia* **2012**, *14*, 1023–1031.
38. Schmiedel, J.; Blaukat, A.; Li, S.; Knochel, T.; Ferguson, K. M. Matuzumab Binding to Egfr Prevents the Conformational Rearrangement Required for Dimerization. *Cancer Cell* **2008**, *13*, 365–373.
39. Kowal, J.; Chami, M.; Baumgartner, P.; Arheit, M.; Chiu, P. L.; Rangl, M.; Scheuring, S.; Schroder, G. F.; Nimigean, C. M.; Stahlberg, H. Ligand-Induced Structural Changes in the Cyclic Nucleotide-Modulated Potassium Channel Mlok1. *Nat. Commun.* **2014**, *5*, No. 3106.
40. Remy, I.; Wilson, I. A.; Michnick, S. W. Erythropoietin Receptor Activation by a Ligand-Induced Conformation Change. *Science* **1999**, *283*, 990–993.
41. Roovers, R. C.; Vosjan, M. J.; Laeremans, T.; El Khoulati, R.; de Bruin, R. C.; Ferguson, K. M.; Verkleij, A. J.; van Dongen, G. A.; van Bergen en Henegouwen, P. M. A Biparatopic Anti-EGFR Nanobody Efficiently Inhibits Solid Tumour Growth. *Int. J. Cancer* **2011**, *129*, 2013–2024.
42. Schmitz, K. R.; Bagchi, A.; Roovers, R. C.; van Bergen en Henegouwen, P. M.; Ferguson, K. M. Structural Evaluation of Egfr Inhibition Mechanisms for Nanobodies/Vhh Domains. *Structure* **2013**, *21*, 1214–1224.
43. Sako, Y.; Minoghchi, S.; Yanagida, T. Single-Molecule Imaging of Egfr Signalling on the Surface of Living Cells. *Nat. Cell Biol.* **2000**, *2*, 168–172.
44. Clayton, A. H.; Orchard, S. G.; Nice, E. C.; Posner, R. G.; Burgess, A. W. Predominance of Activated EGFR Higher-Order Oligomers on the Cell Surface. *Growth Factors* **2008**, *26*, 316–324.
45. Hofman, E. G.; Bader, A. N.; Voortman, J.; van den Heuvel, D. J.; Sigismund, S.; Verkleij, A. J.; Gerritsen, H. C.; van Bergen en Henegouwen, P. M. Ligand-Induced EGF Receptor Oligomerization Is Kinase-Dependent and Enhances Internalization. *J. Biol. Chem.* **2010**, *285*, 39481–39489.
46. Teramura, Y.; Ichinose, J.; Takagi, H.; Nishida, K.; Yanagida, T.; Sako, Y. Single-Molecule Analysis of Epidermal Growth Factor Binding on the Surface of Living Cells. *EMBO J.* **2006**, *25*, 4215–4222.
47. Chung, I.; Akita, R.; Vandlen, R.; Toomre, D.; Schlessinger, J.; Mellman, I. Spatial Control of EGF Receptor Activation by Reversible Dimerization on Living Cells. *Nature* **2010**, *464*, 783–787.
48. Holbro, T.; Civenni, G.; Hynes, N. E. The Erbb Receptors and Their Role in Cancer Progression. *Exp. Cell Res.* **2003**, *284*, 99–110.
49. Behar, G.; Chames, P.; Teulon, I.; Cornillon, A.; Alshoukr, F.; Roquet, F.; Pugniere, M.; Teillaud, J. L.; Gruaz-Guyon, A.; Pelegrin, A.; et al. Llama Single-Domain Antibodies Directed against Nonconventional Epitopes of Tumor-Associated Carcinoembryonic Antigen Absent from Nonspecific Cross-Reacting Antigen. *FEBS J.* **2009**, *276*, 3881–3893.
50. Alvarez-Rueda, N.; Behar, G.; Ferre, V.; Pugniere, M.; Roquet, F.; Gastinel, L.; Jacquot, C.; Aubry, J.; Baty, D.; Barbet, J.; et al. Generation of Llama Single-Domain Antibodies against Methotrexate, a Prototypical Hapten. *Mol. Immunol.* **2007**, *44*, 1680–1690.
51. Even-Desrumeaux, K.; Baty, D.; Chames, P. Strong and Oriented Immobilization of Single Domain Antibodies from Crude Bacterial Lysates for High-Throughput Compatible Cost-Effective Antibody Array Generation. *Mol. BioSyst.* **2010**, *6*, 2241–2248.
52. Mathis, G. Rare Earth Cryptates and Homogeneous Fluoroimmunoassays with Human Sera. *Clin Chem.* **1993**, *39*, 1953–1959.